BMC Neuroscience

RESEARCH

Open Access

A rat model establishment of bronchopulmonary dysplasia-related lung & brain injury within 28 days after birth

Xin Lin[1,2,3†], Meicen Zhou[1,3†] and Hua Wang[1,3*]

Abstract

Purpose Lung injury associated with bronchopulmonary dysplasia (BPD) and its related neurodevelopmental disorders have garnered increasing attention in the context of premature infants. Establishing a reliable animal model is essential for delving into the underlying mechanisms of these conditions.

Methods Newborn rats were randomly assigned to two groups: the hyperoxia-induced BPD group and the normoxia (NO) group. For the BPD group, they were nurtured in a hyperoxic environment with a high oxygen inspired fraction (0.85) from birth until day 14 within 28 days postnatally. In contrast, the NO group consisted of newborn rats that were nurtured in a normoxic environment with a standard oxygen inspired fraction (0.21) for 28 days postnatally. Various pathological sections of both lung and brain tissues were examined. TUNEL staining, immunofluorescence assays, and functional tests were performed, and the results were meticulously analyzed to assess the impact of hyperoxia environments on the developing organs.

Results In the newborn rats of the BPD group, a significant reduction in alveolar number coupled with enlargement was observed, alongside severe fibrosis, collagen deposition, and constriction of bronchi and vascular lumens. This was accompanied by an accumulation of inflammatory cells and a marked deterioration in lung function compared to the NO group ($P < 0.05$). Additionally, a decrease in neuronal count, an increase in neuronal apoptosis, proliferation of neuroglia cells, and demyelination were noted, and poorer performance in the Morris water maze test within the BPD group ($P < 0.05$).

Conclusion The BPD-rats model was established successfully. Lung injury in the BPD group evident across the bronchi to the alveoli and pulmonary vessels, which was associated with deteriorated lung function at postnatal day 14. Concurrently, brain injury extended from the cerebral cortex to the hippocampus, which was associated with impaired performance in orientation navigation and spatial probe tests at postnatal day 28.

Keywords Lung, Brain, BPD, Rat model, Hyperoxia

†Xin Lin and Meicen Zhou contributed equally to this work.

*Correspondence:
Hua Wang
wanghua@scu.edu.cn
[1]Department of Pediatrics, West China Second University Hospital, Sichuan University, Chengdu, China
[2]Department of Neonatology, Fujian Maternity and Child Health Hospital/College of Clinical Medicine for Obstetrics & Gynecology and Pediatrics, Affiliated Hospital of Fujian Medical University, Fuzhou, China
[3]Key Laboratory of Birth Defects and Related Disease of Women and Children (Sichuan University), Ministry of Education, Sichuan University, No. 20, Section 3, South Renmin Road, Chengdu, Sichuan Province 610041, China

Introduction

Bronchopulmonary dysplasia (BPD) is a chronic lung disease that exerts detrimental effects on the development of neonatal lungs, particularly under conditions of prolonged oxygen toxicity, barotrauma, or inflammation. This disease ultimately results in lung injury and significantly influences the incidence and mortality rates of respiratory-related complications [1]. Hyperoxia exposure is a critical factor in the development of BPD, causing direct lung injury through the generation of reactive oxygen species and the recruitment of inflammatory cells [2]. Animal models that mimic hyperoxia-induced lung injury are instrumental in studying the condition in premature infants with BPD [3]. It has been observed in the animal model that maintaining a high fraction of inspired oxygen (FiO2) of 0.85 during the first fourteen days postnatally leads to a reduction in the total number of alveoli and an increase in the thickness next to the alveoli [4]. The hyperoxia group exhibited a decrease in body weight and alveolar count.

[5]. After seven days of hyperoxia exposure, alterations in micro-CT barium contrast and pulmonary artery media thickness were observed [6]. The lung injury associated with BPD could be mitigated by dampening the inflammatory response and fibrosis triggered by hyperoxia [7]. However, existing studies have not yet provided a comprehensive analysis of hyperoxia-induced lung injury [8, 9], particularly regarding the structural changes that span from the bronchi to the alveoli and the extent of fibrosis. Furthermore, infants with BPD would be at risk for neurodevelopmental disorders [10, 11], and impaired brainstem myelination and synaptic function were evoked by auditory brainstem responses in very preterm infants [12]. The potential detrimental effects of BPD on white matter and cerebellar development have been documented through regional brain volume assessments and diffusion tensor imaging using MRI [13]. Additionally, the Webster scale indicated that children with BPD exhibited a diminished processing speed quotient, reflecting poorer cognitive performance [14]. Newborn mice were particularly susceptible to immature neuronal damage and white matter myelination disorders when subjected to chronic hyperoxia [15, 16].

As the absence of a reliable BPD-rat model that elucidates the specific sites and mechanisms of injury within the lung and brain, we developed a model that incorporates hyperoxia exposure for twenty-eight days postnatally to investigate these aspects more comprehensively.

Materials and methods

Animal model

All animal procedures were conducted according to the Declaration of ARRIVE guidelines and approved by the Experimental Animal Management and Ethics Committee of the West China Second University Hospital, Sichuan University (2023074). Parturient Sprague Dawley (SD) rats (D000017, wt/wt) were transferred from Laboratories (Gem Pharmatech Co., Ltd) to the Key Laboratory of Birth Defects and Related Disease of Women and Children in Sichuan University. Pregnant SD rats and their neonatal offspring were nurtured under standard conditions, with free access to food and water, at a temperature of 25–28 °C and a humidity of 55–65%. They were randomly assigned to two groups: (1) the normoxia (NO) group, which was nurtured in ambient air with a FiO2 of 0.21; and (2) the hyperoxia-induced BPD group, which was nurtured in a high-oxygen environment with an FiO2 of 0.85, an oxygen flow rate of 1.5 l/min, CO_2 levels below 0.5%, and humidity maintained at 55–65% using an atmospheric pressure chamber (Hangzhou Ai-pu Co., Ltd.). To prevent hyperoxia-induced damage to the mothers [17], their mothers were alternated daily between cages starting from the first day postpartum (P1, equivalent to 23–32 weeks of human gestational age) [18], until the fourteenth day (P14, equivalent to one month of human age which was recognized as the maturity period for the BPD lung injury model [4]) [19, 20]. Newborn rats were nurtured until the twenty-eighth day postnatally (P28), which corresponded to six months of age in preterm human being infants [21], and their weights were recorded at six time points (P1, P3, P7, P14, P21, P28) at 9:00 a.m. daily (sfigure 1). After being anesthetized with inhaled isoflurane (1.5-3%, 100 ml), the rats were perfused with 0.01mmol/l phosphate-buffered saline at a constant pressure of 20 cm H_2O [22], and their left lobe lungs and whole brains were then fixed in 4% paraformaldehyde for subsequent histopathological analysis.

Hematoxylin-eosin (H&E) staining

The paraffin-embedded lung and brain sections were uniformly cut to a thickness of 3 μm slices and stained with hematoxylin, differentiation solution and eosin reagent (Servicebio, China), dehydrated with 100% ethanol and n-butanol, infiltrated with xylene, and then sealed with neutral resin. Lung slices were analyzed on the six structures: bronchia, bronchiole, terminal bronchiole, respiratory bronchiole, pulmonary vessel, and alveolus (Fig. 1). Brain slices were analyzed in three regions: cerebral cortex, corpus callosum and hippocampus (Fig. 2).

Masson staining

Paraffin-embedded lung sections were divided into upper, middle, and lower fields, and each field, with a thickness of 4 μm and an area of 25 μm^2, was stained using the Masson dye solution set (Servicebio, China). The staining process included treatment with 1% glacial acetic acid, dehydration with anhydrous ethanol, and

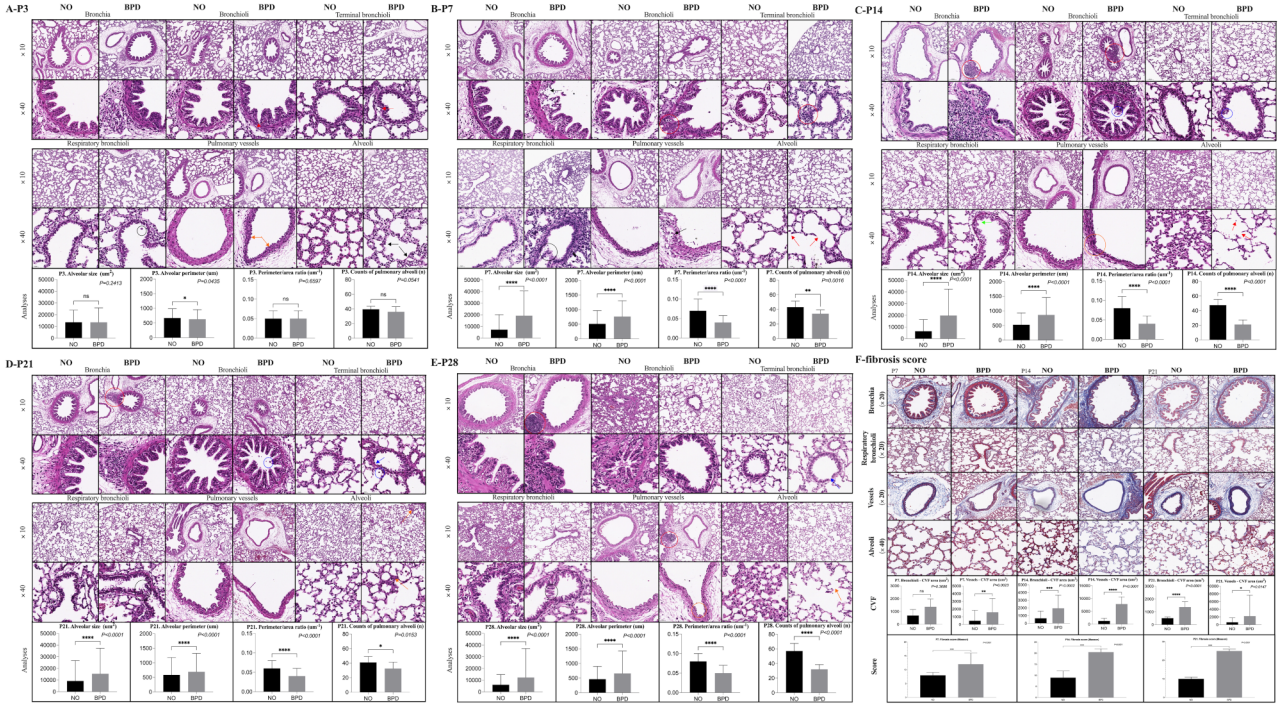

Fig. 1 Pathological lung structures from P3 to P28, and collagen volume fraction (CVF) areas indicating fibrosis from P7 to P21

soaking in 100% ethanol and Xylene, followed by sealing with neutral gum. The field score (sfigure 2) was determined according to the criteria established by Hübner et al. [23]. When it was challenging to differentiate between two odd-numbered grades, an intervening even-numbered score was assigned. The predominant degree of alveolar fibrosis was recorded as the one occupying more than half of the field area.

Nissl staining

Paraffin-embedded brain sections, each precisely cut to a thickness of 3 μm, were stained with Toluidine Blue dye solution (Servicebio, China) and then slightly differentiated with 0.1% glacial acetic acid (SCRC, China). The degree of differentiation was carefully controlled under a microscope (LEICA, Germany) to ensure optimal staining results.

Luxol fast Blue (LFB) staining

Paraffin-embedded brain sections, each precisely cut to a thickness of 3 μm, were stained with LFB staining kit (Servicebio, China), counterstained in 95% ethanol and Eosin (Servicebio, China), and then sealed with neutral gum. The demyelination degrees in the cerebral cortex, corpus callosum, and hippocampal CA1 region was assessed through LFB staining [24] at P7, P14, and P21 (Fig. 2).

TUNEL staining

After dewaxing in xylene, the paraffin-embedded brain slices (a thickness of 3 μm) were treated with DNase-free proteinase K (20 μg/ml) at room temperature, followed by a one-hour incubation with TUNEL working solution at 37 °C in the dark. DAPI Fluoromount-G™ [Sigma] was then applied for counterstaining, as shown in Fig. 2d [25, 26].

Immunofluorescence assay

The paraffin-embedded hippocampal slices (a thickness of 3 μm) were permeabilized with 0.5% Triton X-100, incubated in a blocking solution before being incubated to primary and secondary antibody. The primary antibodies were incubated for twenty-four hours at 4 °C [27], targeting specific cell types as follows: microglial cells were stained with IBA-1 marker (Abcam, ab283319, 1:500, Mouse), oligodendrocytes were stained with SOX-10 marker (Abcam, ab227680, 1:500, Rabbit), astrocytes were stained with GFAP marker (Abcam, ab7260, 1:1000, Rabbit), and neurons were stained with NeuN marker (Abcam, ab104224, 1:500, Mouse). The secondary antibody used was Alexa 488-conjugated anti-rabbit IgG (Vector Laboratories Inc., Burlingame, CA, USA) to bind the rabbit primary antibody, and HA 594-conjugated anti-mouse IgG (HA1126) to bind the mouse primary antibodies.

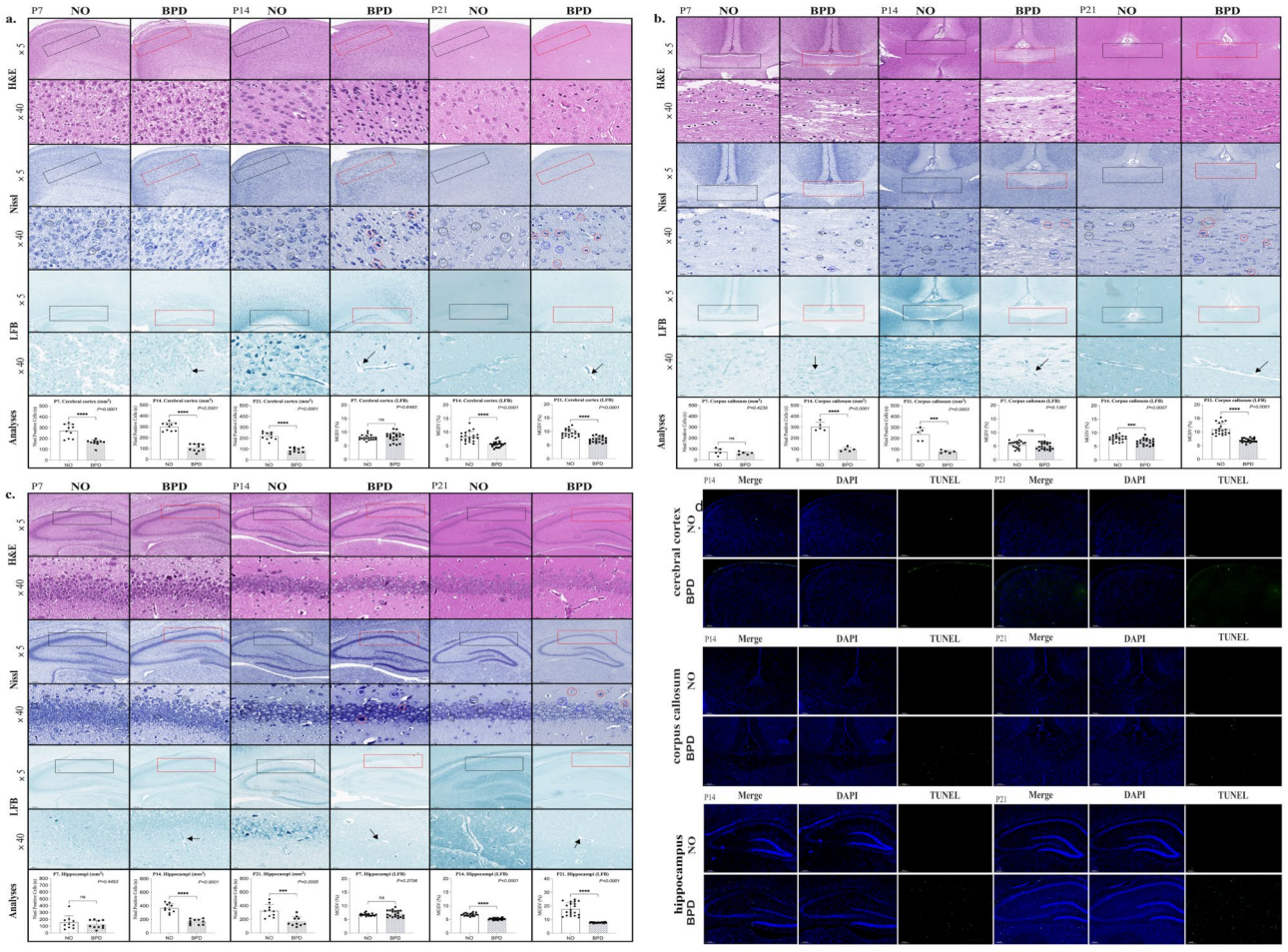

Fig. 2 Pathological brain sections of cerebral cortex, corpus callosum and hippocampus (**a-c**) and TUNEL-staining for apoptotic cells from P14 to P21 (**d**)

Lung function test

The lung function of newborn rats at P14, totaling twenty-two subjects in each group, was assessed using a Respiratory Function System (FinePointe RC, Wilmington, NC, USA) for a duration exceeding three minutes [28]. The targeted parameters for analysis included respiratory rate (f), tidal volume (TV), minute ventilation (MV), functional residual capacity (FRC), specific airway resistance (sRaw), specific airway conductance (sGaw), peak inspiratory flow (PIF), peak expiratory flow (PEF), inspiratory time (Ti), expiratory time (Te), the timing of the peak expiratory flow as a fraction of Te (Rpef), and expiratory flow at 50% of expired volume (EF50) [29], as shown in Fig. 3A.

Morris water maze test

Each group of ten newborn rats underwent training for once in the acquisition sessions (one trials per day from the first to fourth quadrant in turn interval twenty-four hours) to locate a submerged transparent resin platform within a circular pool covered by black curtains around (diameter: 150 cm, wall depth: 50 cm, water temperature: 24±2 °C). Rats that failed to locate the platform within 90s were manually placed on the platform and allowed to stay for 15s to familiarize themselves with the location. The orientation navigation test, which tracked the latency and distance to the targeted platform, was conducted from the 1st to the 6th day (90s per trial, with the platform remaining in place). On the 6th day, a spatial probe test was also administered, which measured the distance in critical quadrant, entries in critical quadrant, and time in critical quadrant (90s, platform with the platform removed). These tests were monitored and recorded using a video-tracking system (Panlab SMART 3.0) [30, 31], as shown in Fig. 3B.

Statistical analyses

The statistical analyses were performed using SPSS Statistics version 27.0 (IBM Corp, Armonk, NY, USA). If fit to a normal distribution, the variables were analyzed by t-tests; if not, they were analyzed by the Mann-Whitney U test. All slices were scanned by MIDI (Pannoramic 3DHISTECH, Hungary). The area, perimeter, perimeter/area ratio and counts of alveoli were quantified in

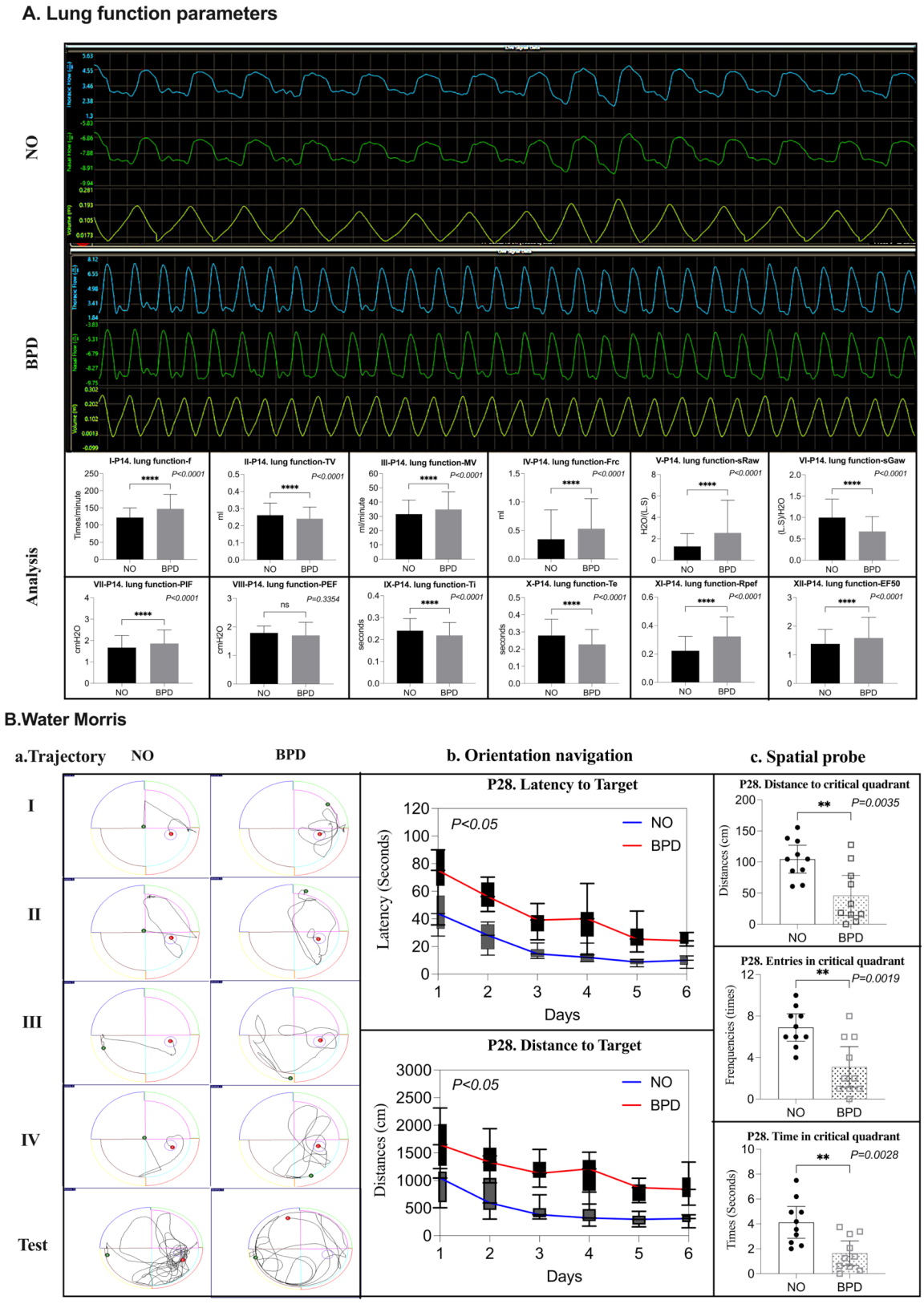

Fig. 3 The lung function parameters in P14 and the Morris water maze in P28

(μm^2), (μm), (μm^{-1}), and (n). The collagen volume fraction (CVF) areas of fibrosis [32] and positive cells were counted with Image J or Image Pro (Ruichi Technology, China), and their diagrams were visualized by Graph prism 10. Five consecutive but non-overlapping field of vision (magnification of 40×) were randomly selected in the hippocampal CA1, CA2, CA3, and dentate gyrus (DG) regions, the external granular regions of cerebral cortex, and the corpus callosum regions. The Nissl's bodies or fluorescent positive cells and demyelination degrees (Mean Gray Scale Value, MGSV) from these areas were analyzed and presented [33]. $P < 0.05$ were considered statistically significant.

Results

We successfully replicated the establishment of a BPD-related brain injury model twice, with newborn rats divided into a control group (NO group) and a model group (BPD group) for each experimental run, as shown in Fig. 4. The newborn rats in the BPD group exhibited a significantly poorer weight gain tendency compared to those in the NO group (sfigure 1).

In the bronchia, the structure of pseudostratified ciliated epithelial cells fragmented, and the cavity became deformed. In the bronchioles and terminal bronchioles, the monolayer ciliated columnar epithelial cells exhibited disorder, with the basal layer even becoming exposed externally. The epithelial cells shedding occurred, leading to vacuole formation and obstruction of the bronchial lumen within the respiratory bronchioles. The vascular cavity constricted, vascular smooth muscle tissues loosened, and collagen fibers were deposited alongside, with fractures and stratifications evident. Pulmonary vascular endothelial cells underwent detachment and morphological changes from a flat cuboidal shape to a smoother form. The alveolar cavity began to expand from P3, with walls thinning and even rupturing. Alveolar septal fibrosis hyperplasia and irregular flake fibrosis structures emerged locally. Alveolar ectasia was pronounced, with evident fractures and stratifications. An aggregation of inflammatory cells encircled the bronchia, bronchioles, and terminal bronchioles (Fig. 1). The BPD group exhibited larger alveolar size and perimeter, smaller perimeter/area ratio, and reduced alveolar counts from P7 to

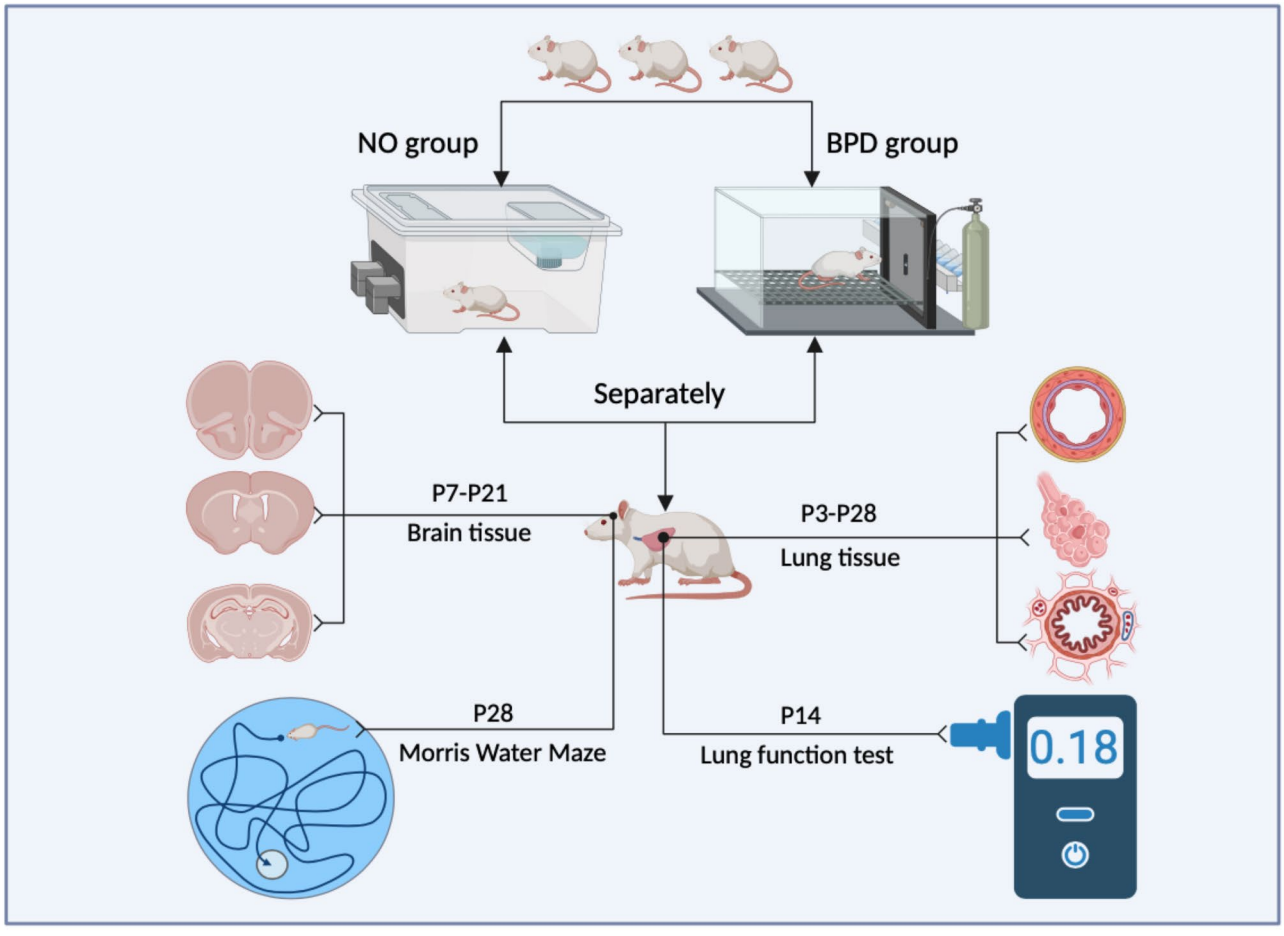

Fig. 4 The flow diagram on BPD-related brain injury model for newborn rats from P1 to P28 after birth

P28 ($P < 0.05$). The standard score of alveolar fibrosis was presented in sfigure 2, showing that the fibrosis degree worsened from P7, peaked at P21, and was concentrated around the bronchioles and vessels in the BPD group (Fig. 1F). Except for the PEF of lung function results ($P = 0.332$), P14-rats in the BPD group displayed higher f, MV, Frc, sRaw, PIF, Rpef and EF50, along with lower TV, sGaw, Ti and Te compared to those in the NO group ($P < 0.05$), as shown in Fig. 3A.

Neurons in the extracerebral granular regions of the cerebral cortex and hippocampal CA1 regions exhibited disordered polar arrangement, with nuclei solidifying and cytoplasmic vacuolation occurring. As the myelin sheath of neurons broken down, significant demyelination changes, indicated by a lower MGSV, were observed. The fibers of the cerebral cortex, corpus callosum and hippocampal regions were sparsely arranged and left empty, and their MGSV decreased in the BPD group at P14 and P21 ($P < 0.05$), as shown in Fig. 2a-c. The Nissl's bodies (normal cells) were dissolved, and decreased in the cerebral cortex, corpus callosum and hippocampal CA1 regions. Cells with karyopyknotic changes (blue circle) or completely dissolved nuclei (red circle) were considered to have negative Nissl's bodies in both groups, whereas neurons with fully contained cytoplasm and intact nuclei in Nissl staining were defined as positive cells (black circle). At P7, there were no differences in Nissl-positive cells between the two groups in the corpus callosum and hippocampal regions ($P > 0.05$), except in cerebral cortex regions ($P < 0.001$). However, the number of Nissl-positive cells in different brain regions of the BPD group was significantly lower than that in the NO group at both P14 and P21 ($P < 0.05$). Apoptotic neurons, stained by TUNEL, were predominantly observed in the three brain regions of the BPD group, with virtually no neuronal apoptosis detected in the NO group (Fig. 2d). When we examined the whole brain specimens from rats, we had removed the meninges that envelop the brain tissue. Consequently, we believe that the TUNEL-positive cells observed in the cortical or hippocampal border regions are likely false positives. These were attributed to the peripheral effects of fluorescent staining, as confirmed under a fluorescence microscope.

In the BPD group, there was a notable reduction in the counts of neurons, conversely, an increase was observed in the numbers of astrocytes and microglial cells, as shown in Fig. 5a, b. The hippocampal CA1, CA2, and CA3 regions exhibited a significant upsurge in the numbers of microglial cells and astrocytes in the BPD group ($P < 0.05$), and the BPD group showed a diminished number of fluorescent neurons compared to the NO group within the hippocampal CA1 and CA2 regions ($P < 0.05$), as shown in Fig. 5c.

The Morris water maze test was conducted on P28-rats to assess their orientation navigation and spatial probe abilities (Fig. 3B). Throughout the entire 6-day training period, the BPD group exhibited significantly longer distances and latency times to reach the targeted platform ($P < 0.05$). On the 6th day, when the platform was removed, the BPD group also demonstrated shorter distances, fewer entries, and less time spent in the critical quadrant compared to the NO group ($P < 0.05$).

Discussion

Our findings indicated that lung injury began to manifest from the 7th day, while BPD-related brain injury became evident from the 14th day. In the BPD-model rats, pulmonary vascular endothelial cells shed, leading to a narrowing of the vascular lumen, deposition of collagen fibers, and relaxation of vascular smooth muscle. The presence of larger but fewer alveoli and heightened inflammatory cell infiltration helped to explain the poorer lung function results observed in P14-rats. The reduction in neuronal count, proliferation of neuroglia cells, and demyelination of the myelin sheath account for the impaired orientation navigation and spatial probe abilities in P28-rats.

Lung injury

Newborn rats were utilized in our study for their stage of lung development is analogous to that of preterm infants, and their lungs were in a cystic phase at birth, a period that extends from embryonic day (E18.5) to the 5th day postnatally [34]. We observed an increase in alveolar simplification in rats exposed to hyperoxia from P7 to P14, a finding that aligns with existing literature [35]. In our study, an enlargement in alveolar size and perimeter, coupled with a reduction in alveolar counts, persisted in the rats from P14 to P28. The alveolar fibrosis was most severe in P21-rats, which is consistent with the gas exchange dysfunction observed in BPD infants [36]. Additionally, we detected collagen fiber deposition surrounding bronchioles and blood vessels in the BPD group, a result of hyperoxia-activated renin-angiotensin system [37].

The expansion of alveoli resulted in an increase in Frc and a decrease in TV. To achieve more effective ventilation and maintain the body's oxygen supply, the f increased, which was reflected in shorter Ti and Te times, and a corresponding increase in MV appropriately. As fibrosis worsened, with increased collagen deposition and inflammatory cell infiltration, pulmonary airway resistance rose, characterized by high values of PIF, sRaw, and EF50, along with low sGaw, further exacerbating lung injury [38–40]. These manifestations were indicative of obstructive and restrictive ventilatory dysfunctions associated with BPD [41]. Prolonged exposure to

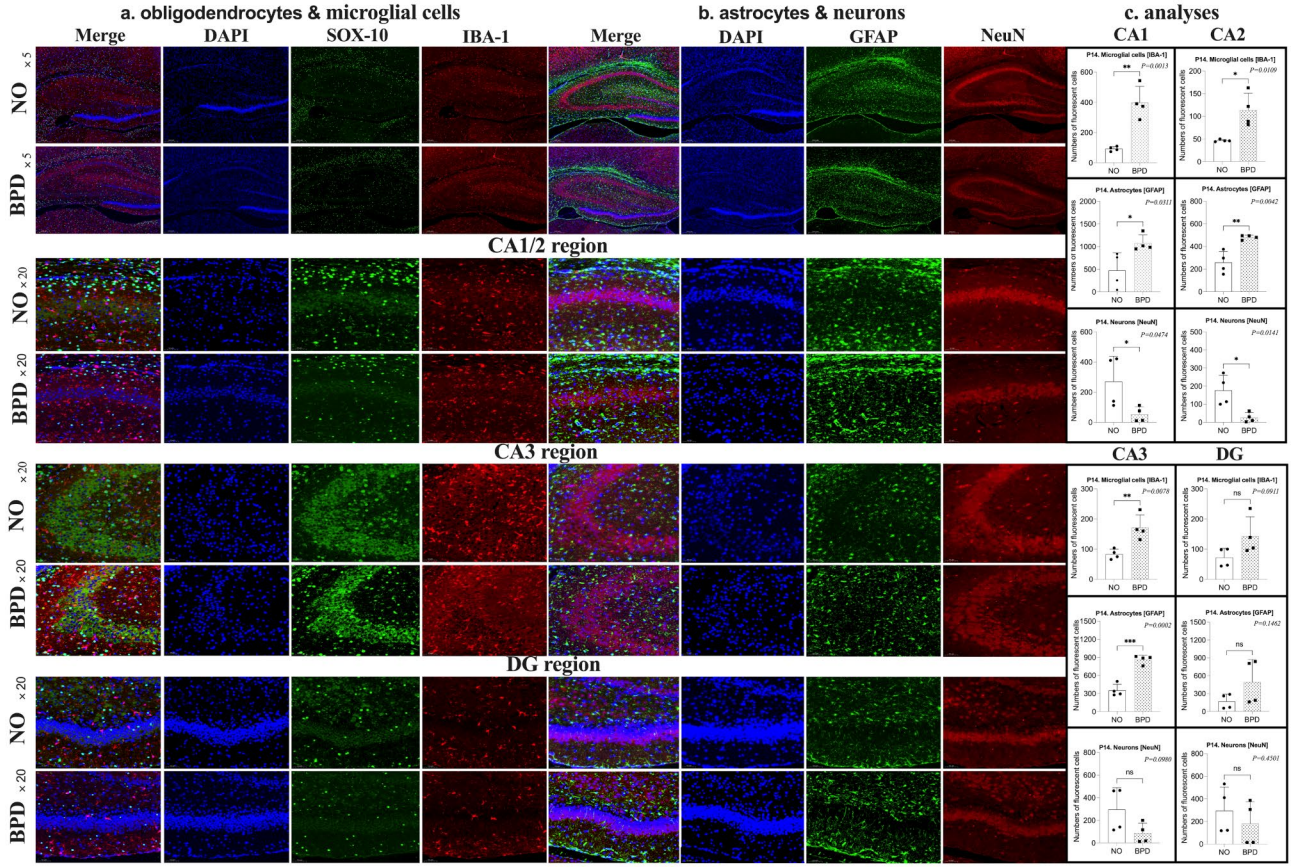

Fig. 5 Fluorescent staining (**a-b**) oligodendrocytes (SOX-10), astrocytes (GFAP), microglial cells (IBA-1), and neurons (NeuN) and numbers of them (**c**) in different hippocampal regions (CA1, CA2, CA3 and DG) in P14

hyperoxia can lead to persistent pulmonary hypertension due to the influx of inflammatory cells and pulmonary vascular remodeling [42, 43]. Vascular endothelial growth factor, as a key factor in vascular development, showed decreased expression in BPD infants, attributed to the abnormal formation of alveolar microvessels [44].

BPD-related brain injury

Hyperoxia was found to activate circulating extracellular vehicles (EVs) in newborn BPD-rats. These EVs increased the levels of surfactant protein, which contributed to brain injury [45]. The activation of the inflammasome led to an upregulation in the production of mature IL-1β, highlighting the inflammasome's pivotal role in hyperoxia-induced lung and brain injury in neonates [46]. We observed a reduction in neuronal count and a rise in neuronal apoptosis within the cerebral cortex, corpus callosum, and hippocampal regions. The demyelination of the myelin sheath happened in all three regions from P14 to P21, and it was particularly pronounced in the corpus callosum regions. The presence of oxidative stress, neutrophilic infiltration, and mitochondrial respiratory chain enzymes in the hippocampus and prefrontal cortex can account for these findings [47]. BPD was one of the six factors contributing to the reduction in microstructural integrity or development in the corpus callosum regions during the first six months following very preterm birth [48]. The decreased myelination in the corpus callosum may stem from vascular occlusion and subsequent ischemia [49]. The neuronal apoptosis and demyelination of the myelin sheath detected in the hippocampus were linked to the impaired directional navigation and spatial probe abilities.

Astrocytes reacted to pathological stimuli through a process known as "reactive astrogliosis," and an increase in cortical astrocytes had been documented following hyperoxia [50]. Similarly, we identified an upregulation of astrocytes in the hippocampus, which we believe was indicative of reactive inflammation in our study. Microglial cells are involved in regulating astrocyte activity, and astrocytes also influence microglial responses during central nervous system inflammation [51]. Consistent with this interaction, our study also revealed an increase in microglial cells within the hippocampus.

Limitations

Our current study did not delve into the signaling pathways that link lung and brain injuries following hyperoxia, which represents an important direction for our upcoming research endeavors. Moreover, while we examined the alterations in neurons and glial cells, we have yet to conduct a thorough analysis of specific protein expressions and markers. This is an area we intend to further investigate and complete in our future studies.

Conclusion

The BPD-rats model was established successfully. Lung injury in the BPD group evident across the bronchi to the alveoli and pulmonary vessels, which was associated with deteriorated lung function at postnatal day 14. Concurrently, brain injury extended from the cerebral cortex to the hippocampus, which was associated with impaired performance in orientation navigation and spatial probe tests at postnatal day 28.

Abbreviations

BPD	Bronchopulmonary dysplasia
CVF	Collagen volume fraction
DG	Dentate gyrus
EF50	Expiratory flow at 50% of expired volume
EVs	Extracellular vehicles
f	Respiratory rate
FiO2	Fraction of inspired oxygen
FRC	Functional residual capacity
H&E	Hematoxylin-eosin
LFB	Luxol Fast Blue (LFB)
MV	Minute ventilation
MGSV	Mean Gray Scale Value
NO	Normoxia
PEF	Peak expiratory flow
PIF	Peak inspiratory flow
Rpef	The timing of the peak expiratory flow as a fraction of Te
sRaw	Specific airway resistance
sGaw	Specific airway conductance
SD	Sprague Dawley
TV	Tidal volume
Ti	Inspiratory time
Te	Expiratory time

Supplementary Information

The online version contains supplementary material available at https://doi.org/10.1186/s12868-024-00912-w.

Supplementary sFigure 1: The tendency of weight for newborn rats from P1 to P28 after birth in the BPD and NO group

Supplementary sFigure 2: The standard score of the alveolar fibrosis

Supplementary Material 3

Supplementary Material 4

Supplementary Material 5

Supplementary Material 6

Supplementary Material 7

Supplementary Material 8

Supplementary Material 9

Supplementary Material 10

Supplementary Material 11

Supplementary Material 12

Supplementary Material 13

Supplementary Material 14

Supplementary Material 15

Acknowledgements

The authors want to thank the Heads of Neonatal Department, Fujian Maternity and Child Health Hospital & West China Second University Hospital, Key Laboratory of Birth Defects and Related Disease of Women and Children (Sichuan University) for their permission and support the study.

Author contributions

All authors edited the manuscript and read and approved the final manuscript. X Lin and H Wang contributed to the development of the experimental design. X Lin performed laboratory experiments. X Lin and M Zhou analyzed the data. X Lin wrote the manuscript.

Funding

This work was supported by the National Natural Science Foundation of China (82241036), Sichuan Provincial Department of Science and Technology central guided local project (2023ZYD0122), and Science and Technology Department of Sichuan Province (23ZYZYTS0099).

Data availability

No datasets were generated or analysed during the current study.

Declarations

Ethics approval and consent to participate

All the operations followed the National Institutes of Health Guidelines for the Care and Use of Laboratory Animals and ARRIVE Guidelines pertaining to animal experimentation. The protocol for all animal experiments was approved (2023074) by the Experimental Animal Management and Ethics Committee of the West China Second University Hospital, Sichuan University (Sichuan, China).

Consent for publication

Not applicable. Availability of data and material.

Competing interests

The authors declare no competing interests.

Received: 31 July 2024 / Accepted: 19 November 2024
Published online: 28 November 2024

References

1. Silva DM, Nardiello C, Pozarska A, Morty RE. Recent advances in the mechanisms of lung alveolarization and the pathogenesis of bronchopulmonary dysplasia. Am J Physiol Lung Cell Mol Physiol. 2015;309(11):L1239–72. https://doi.org/10.1152/ajplung.00268.2015
2. Bhandari V. Hyperoxia-derived lung damage in preterm infants. Semin Fetal Neonatal Med. 2010;15(4):223–9. https://doi.org/10.1016/j.siny.2010.03.009
3. O'Reilly M, Thébaud B. Animal models of bronchopulmonary dysplasia. The term rat models. Am J Physiol Lung Cell Mol Physiol. 2014;307(12):L948–58. https://doi.org/10.1152/ajplung.00160.2014
4. Nardiello C, Mižíková I, Silva DM, Ruiz-Camp J, Mayer K, Vadász I, Herold S, Seeger W, Morty RE. Standardisation of oxygen exposure in the development of mouse models for bronchopulmonary dysplasia. Dis Model Mech. 2017;10(2):185–96. https://doi.org/10.1242/dmm.027086
5. Zhang X, Chu X, Weng B, Gong X, Cai C. An innovative model of bronchopulmonary dysplasia in premature infants. Front Pediatr. 2020;8:271. https://doi.org/10.3389/fped.2020
6. Hara T, Shimbo T, Masuda T, Kitayama T, Fujii M, Hanawa M, Yokota K, Endo M, Tomimatsu T, Kimura T, Tamai K. High-mobility group box-1 peptide

ameliorates bronchopulmonary dysplasia by suppressing inflammation and fibrosis in a mouse model. Biochem Biophys Res Commun. 2023;671:357–65. https://doi.org/10.1016/j.bbrc.2023.06.032
7. Jiménez J, Richter J, Nagatomo T, Salaets T, Quarck R, Wagennar A, Wang H, Vanoirbeek J, Deprest J, Toelen J. Progressive vascular functional and structural damage in a bronchopulmonary dysplasia model in Preterm rabbits exposed to Hyperoxia. Int J Mol Sci. 2016;17(10):1776. https://doi.org/10.3390/ijms17101776
8. Pan YQ, Hou AN. Hyperoxia-induced lung injury increases CDKN1A levels in a newborn rat model of bronchopulmonary dysplasia. Exp Lung Res 2018 Oct-Nov;44(8–9):424–32. https://doi.org/10.1080/01902148.2018.1479898
9. Cetinkaya M, Cansev M, Kafa IM, Tayman C, Cekmez F, Canpolat FE, Tunc T, Sarici SU. Cytidine 5'-diphosphocholine ameliorates hyperoxic lung injury in a neonatal rat model. Pediatr Res. 2013;74(1):26–33. https://doi.org/10.1038/pr.2013.68
10. Gou X, Yang L, Pan L, Xiao D. Association between bronchopulmonary dysplasia and cerebral palsy in children: a meta-analysis. BMJ Open. 2018;8(9):e020735. https://doi.org/10.1136/bmjopen-2017-020735
11. DeMauro SB. Neurodevelopmental outcomes of infants with bronchopulmonary dysplasia. Pediatr Pulmonol. 2021;56(11):3509–17. https://doi.org/10.1002/ppul.25381
12. Wilkinson AR, Brosi DM, Jiang ZD. Functional impairment of the brainstem in infants with bronchopulmonary dysplasia. Pediatrics. 2007;120(2):362–71. https://doi.org/10.1542/peds.2006-3685
13. Lee JM, Choi YH, Hong J, Kim NY, Kim EB, Lim JS, Kim JD, Park HK, Lee HJ. Bronchopulmonary dysplasia is Associated with altered brain volumes and White Matter Microstructure in Preterm infants. Neonatology. 2019;116(2):163–70. https://doi.org/10.1159/000499487
14. de Mello RR, Rodrigues Reis AB, da Silva KS. Cognitive performance of premature infants: association between bronchopulmonary dysplasia and cognitive skills. Cross-sectional study. Sao Paulo Med J. 2017 Jul-Aug;135(4):383–90. https://doi.org/10.1590/1516-3180.2017.0010190317
15. Chen W, Wang R, Chen C. Cerebral myelination in a Bronchopulmonary Dysplasia Murine Model. Child (Basel). 2023;10(8):1321. 10.3390/children10081321.
16. Lithopoulos MA, Toussay X, Zhong S, Xu L, Mustafa SB, Ouellette J, Freitas-Andrade M, Comin CH, Bassam HA, Baker AN, Sun Y, Wakem M, Moreira AG, Blanco CL, Vadivel A, Tsilfidis C, Seidner SR, Slack RS, Lagace DC, Wang J, Lacoste B, Thébaud B. Neonatal hyperoxia in mice triggers long-term cognitive deficits via impairments in cerebrovascular function and neurogenesis. J Clin Invest. 2022;132(22):e146095. https://doi.org/10.1172/JCI146095
17. Han W, Li X, Zhang H, et al. Recombinant human elafin promotes alveologenesis in newborn mice exposed to chronic hyperoxia. INT J BIOCHEM CELL B. 2017;92:173–82. https://doi.org/10.1016/j.biocel.2017.08.004
18. Back S, Luo N, Borenstein N, et al. Late oligodendrocyte progenitors coincide with the Developmental window of vulnerability for human perinatal White Matter Injury. J NEUROSCI. 2001;21(4):1302–12. https://doi.org/10.1523/jneurosci.21-04-01302.2001
19. Ali M, Heyob K, Tipple TE, Pryhuber GS, Rogers LK. Alterations in VASP phosphorylation and profilin1 and cofilin1 expression in hyperoxic lung injury and BPD. Respir Res. 2018;19(1):229. https://doi.org/10.1186/s12931-018-0938-1
20. Jia D, Zheng J, Zhou Y, Jia J, Ye X, Zhou B, Chen X, Mo Y, Wang J. Ferroptosis is involved in Hyperoxic Lung Injury in neonatal rats. J Inflamm Res. 2021;14:5393–401. https://doi.org/10.2147/JIR.S335061
21. Dutta S, Sengupta P. Men and mice: relating their ages. Life Sci. 2016;152:244–8. https://doi.org/10.1016/j.lfs.2015.10.025
22. Burkhardt W, Kraft S, Ochs M, Proquitté H, Mense L, Rüdiger M. Persurf, a new method to improve surfactant delivery: a study in surfactant depleted rats. PLoS ONE. 2012;7(10):e47923. https://doi.org/10.1371/journal.pone.0047923
23. Hübner RH, Gitter W, El Mokhtari NE, Mathiak M, Both M, Bolte H, Freitag-Wolf S, Bewig B. Standardized quantification of pulmonary fibrosis in histological samples. Biotechniques. 2008;44(4):507–11. https://doi.org/10.2144/000112729
24. Xue R, Pan S, Guo D. Effect of hyperbaric oxygen on myelin injury and repair after hypoxic-ischemic brain damage in adult rat. Neurosci Lett. 2023;794:137015. https://doi.org/10.1016/j.neulet.2022.137015
25. Wei S, Chen F, Xu T, Cao M, Yang X, Zhang B, Guo X, Yin D. BDE-99 disrupts the photoreceptor patterning of zebrafish larvae via transcription factor six7. Environ Sci Technol. 2022;56(9):5673–83. https://doi.org/10.1021/acs.est.1c08914
26. Li Y, Sun S, Wen C, Zhong J, Jiang Q. Effect of Enterococcus faecalis OG1RF on human calvarial osteoblast apoptosis. BMC Oral Health. 2022;22(1):279. https://doi.org/10.1186/s12903-022-02295-y
27. Yoo YM, Jung EM, Jeung EB, Jo BR, Joo SS. Amylin Protein Expression in the rat brain and Neuro-2a cells. Int J Mol Sci. 2022;23(8):4348. https://doi.org/10.3390/ijms23084348
28. Zhu FF, Wang YM, He GZ, Chen YF, Gao YD. Different effects of acetyl-CoA carboxylase inhibitor TOFA on airway inflammation and airway resistance in a mice model of asthma. Pharmacol Rep. 2020;72(4):1011–20. https://doi.org/10.1007/s43440-019-00027-8
29. Condor Capcha JM, Kamiar A, Robleto E, Saad AG, Cui T, Wong A, Villano J, Zhong W, Pekosz A, Medina E, Cai R, Sha W, Ranek MJ, Webster KA, Schally AV, Jackson RM, Shehadeh LA. Growth hormone-releasing hormone receptor antagonist MIA-602 attenuates cardiopulmonary injury induced by BSL-2 rVSV-SARS-CoV-2 in hACE2 mice. Proc Natl Acad Sci U S A. 2023;120(48):e2308342120. https://doi.org/10.1073/pnas.2308342120
30. Saroja SR, Sase A, Kircher SG, Wan J, Berger J, Höger H, Pollak A, Lubec G. Hippocampal proteoglycans brevican and versican are linked to spatial memory of Sprague-Dawley rats in the morris water maze. J Neurochem. 2014;130(6):797–804. https://doi.org/10.1111/jnc.12783
31. Duan H, Zhao S, Xiang J, Ju C, Chen X, Gramaglia I, Yan X. Targeting the CD146/Galectin-9 axis protects the integrity of the blood-brain barrier in experimental cerebral malaria. Cell Mol Immunol. 2021;18(10):2443–54. https://doi.org/10.1038/s41423-020-00582-8
32. Qu S, Shan L, Chen X, Zhang Z, Wu Y, Chen Y, Zhuo F, Wang Y, Dong H. The role of rhIGF-1/BP3 in the prevention of pulmonary hypertension in bronchopulmonary dysplasia and its underlying mechanism. BMC Pulm Med. 2023;23(1):209. https://doi.org/10.1186/s12890-023-02498-1
33. Wang X, Zhang J, Wang S, Song Z, Sun H, Wu F, Lin X, Jin K, Jin X, Wang W, Lin Q, Wang F. Berberine modulates gut microbiota to attenuate cerebral ferroptosis induced by ischemia-reperfusion in mice. Eur J Pharmacol. 2023;953:175782. https://doi.org/10.1016/j.ejphar.2023.175782
34. Morrisey EE, Hogan BL. Preparing for the first breath: genetic and cellular mechanisms in lung development. Dev Cell. 2010;18(1):8–23. https://doi.org/10.1016/j.devcel.2009.12.010
35. Cox AM, Gao Y, Perl AT, Tepper RS, Ahlfeld SK. Cumulative effects of neonatal hyperoxia on murine alveolar structure and function. Pediatr Pulmonol. 2017;52(5):616–24. https://doi.org/10.1002/ppul.23654
36. Bhandari A, Bhandari V. Pathogenesis, pathology and pathophysiology of pulmonary sequelae of bronchopulmonary dysplasia in premature infants. Front Biosci. 2003;8:e370–80. https://doi.org/10.2741/1060
37. Jiang JS, Lang YD, Chou HC, Shih CM, Wu MY, Chen CM, Wang LF. Activation of the renin-angiotensin system in hyperoxia-induced lung fibrosis in neonatal rats. Neonatology. 2012;101(1):47–54. https://doi.org/10.1159/000329451
38. Vanhaverbeke K, Slaats M, Al-Nejar M, Everaars N, Snoeckx A, Spinhoven M, El Addouli H, Lauwers E, Van Eyck A, De Winter BY, Van Hoorenbeeck K, De Dooy J, Mahieu L, Mignot B, De Backer J, Mulder A, Verhulst S. Functional respiratory imaging provides novel insights into the long-term respiratory sequelae of bronchopulmonary dysplasia. Eur Respir J. 2021;57(6):2002110. https://doi.org/10.1183/13993003.02110-2020
39. Durang M, Rigatto H. Tidal volume and respiratory frequency in infants with bronchopulmonary dysplasia (BPD). Early Hum Dev. 1981;5(1):55–62. https://doi.org/10.1016/0378-3782(81)90070-0
40. Vom Hove M, Prenzel F, Uhlig HH, Robel-Tillig E. Pulmonary outcome in former preterm, very low birth weight children with bronchopulmonary dysplasia: a case-control follow-up at school age. J Pediatr. 2014;164(1):40–5. 10.1016/j. jpeds.2013.07.045. e4.
41. Tuková J, Koucký V, Marková D, Koťátko P, Hladíková M, Šulc J. Symptomatic preterm infants suffer from lung function deficits, regardless of bronchopulmonary dysplasia. Pediatr Pulmonol. 2022;57(12):3119–28. https://doi.org/10.1002/ppul.26144
42. Perrone S, Manti S, Buttarelli L, Petrolini C, Boscarino G, Filonzi L, Gitto E, Esposito SMR, Nonnis Marzano F. Vascular endothelial growth factor as Molecular Target for Bronchopulmonary Dysplasia Prevention in very low Birth Weight infants. Int J Mol Sci. 2023;24(3):2729. https://doi.org/10.3390/ijms24032729
43. Alvira CM. Aberrant pulmonary vascular growth and remodeling in Bronchopulmonary Dysplasia. Front Med (Lausanne). 2016;3:21. 10.3389 / fmed.2016.00021.
44. Bhatt AJ, Pryhuber GS, Huyck H, Watkins RH, Metlay LA, Maniscalco WM. Disrupted pulmonary vasculature and decreased vascular endothelial growth factor, Flt-1, and TIE-2 in human infants dying with bronchopulmonary

dysplasia. Am J Respir Crit Care Med. 2001;164(10 Pt 1):1971–80. https://doi.org/10.1164/ajrccm.164.10.2101140
45. Ali A, Zambrano R, Duncan MR, Chen S, Luo S, Yuan H, Chen P, Benny M, Schmidt A, Young K, Kerr N, de Rivero Vaccari JP, Keane RW, Dietrich WD, Wu S. Hyperoxia-activated circulating extracellular vesicles induce lung and brain injury in neonatal rats. Sci Rep. 2021;11(1):8791. https://doi.org/10.1038/s41598-021-87706-w. Erratum in: Sci Rep. 2021;11(1):20229.
46. Dapaah-Siakwan F, Zambrano R, Luo S, Duncan MR, Kerr N, Donda K, de Rivero Vaccari JP, Keane RW, Dietrich WD, Benny M, Young K, Wu S. Caspase-1 inhibition attenuates Hyperoxia-induced lung and Brain Injury in neonatal mice. Am J Respir Cell Mol Biol. 2019;61(3):341–54. https://doi.org/10.1165/rcmb.2018-0192OC
47. Machado RS, Tenfen L, Joaquim L, Lanzzarin EVR, Bernardes GC, Bonfante SR, Mathias K, Biehl E, Bagio É, Stork SS, Denicol T, de Oliveira MP, da Silva MR, Danielski LG, de Quadros RW, Rezin GT, Terra SR, Balsini JN, Gava FF, Petronilho F. Hyperoxia by short-term promotes oxidative damage and mitochondrial dysfunction in rat brain. Respir Physiol Neurobiol. 2022;306:103963. https://doi.org/10.1016/j.resp.2022.103963
48. Teli R, Hay M, Hershey A, Kumar M, Yin H, Parikh NA. Postnatal Microstructural Developmental Trajectory of Corpus Callosum subregions and relationship to clinical factors in very Preterm infants. Sci Rep. 2018;8(1):7550. https://doi.org/10.1038/s41598-018-25245-7
49. Song W, Hoppe G, Hanna D, DeSilva TM, Sears JE. Hyperoxia Induc Hypomyelination Biomedicines. 2022;11(1):37. https://doi.org/10.3390/biomedicines11010037
50. Yin R, Yuan L, Ping L, Hu L. Neonatal bronchopulmonary dysplasia increases neuronal apoptosis in the hippocampus through the HIF-1α and p53 pathways. Respir Physiol Neurobiol. 2016;220:81–7. https://doi.org/10.1016/j.resp.2015.09.011
51. Özer Bekmez B, Tayman C, Çakır U, Koyuncu İ, Büyüktiryaki M, Türkmenoğlu TT, Çakır E. Glucocorticoids in a neonatal hyperoxic lung Injury Model: Pulmonary and neurotoxic effects. Pediatr Res. 2022;92(2):436–44. https://doi.org/10.1038/s41390-021-01777-z

Publisher's note